Domain wall observation and eddy current loss of (110)[001] oriented 17-22 μm thick Si Fe tape wound cores up to 5 kHz

Domain wall observation and eddy current loss of (110)[001] oriented 17–22 μm thick Si-Fe tape-wound cores up to 5 kHz

K. I. Arai, Y. H. Kim, and M. Yamaguchi
Research Institute of Electrical Communication, Tohoku University, Sendai 980, Japan

Dynamic magnetic domain observation and eddy current loss of tape-wound cores are discussed up to 5 kHz. The cores are made of 17–22 μm thick (110)[001] oriented silicon steel strips. Dynamic domain patterns were observed by using SEM on the surfaces of the tape-wound cores. In order to distinguish the moving domain walls from the standing ones, the drive frequency of the core should not be integral multiples of the scan frequency of the SEM(50.0 Hz). The model which includes dynamic wall number, wall bowing, and velocity of each domain wall agreed comparatively well with the measured eddy current losses.

INTRODUCTION

Many works have been performed on the relation between the losses of tape-wound core and dynamic domain behavior.[1,2] However, few works were based on actual dynamic domain observations.

Here, we observed the dynamic domain patterns of toroidal cores using a SEM up to 5 kHz, and studied the dynamic behavior of domains such as the increase of the number of domain walls and the velocity of each domain wall. The correlation of eddy current losses with the observed dynamic behavior of the domains was also discussed.

THE OBSERVATION METHOD OF DYNAMIC DOMAIN PATTERN

The cores are made of 17–22 μm thick (110)[001] oriented silicon steel strips with a high degree of grain orientation.[3-5] The silicon steel strips were wound in quartz glass annealing holders which had inner diameters of either about 12 or 24 mm. Then stress relief annealing was performed at 900 °C for 1 h. The strips used were not coated for tension or insulation. We manufactured 20 cores and here we discuss the typical results obtained for the two cores listed in Table I.

The dynamic domain observations and the loss measurements were performed simultaneously with a core fixture shown in Fig. 1. The core is set in the toroidal holder.

Figure 2 explains the method for observing dynamic domain patterns. The sample is shown in the CRT display of the SEM. When a magnetic field is applied under sinusoidal flux condition, the 180° domain walls move in the sample width direction. The sinusoidal waves in Fig. 2 represent the movement of the domain wall as a function of the position and time. The inclined lines that cross the CRT display represent the scan lines of the SEM. The direction of the scan lines and the 180° domain walls meet at right angles. Because the boundary between adjacent domains appears only when the domain wall line and the scan line cross, the observed dynamic domain pattern looks like a broken line.

Figure 3 shows the photographs and the computer simulations of the dynamic domain pattern which looks like a sawtooth wave. The scan frequency of the SEM was fixed to 50.0 Hz. The photographs of Figs. 3(a)–3(c) correspond to the simulations of Figs. 3(d)–3(f), respectively, and they agree very well. When the drive frequency equals the scan frequency or its integral multiples, the observed dynamic domain pattern becomes like a static one as shown in Fig. 3(a). If there is any difference between the drive frequency and the scan frequency, a sawtooth dynamic domain pattern is obtained and the number of teeth in the sawtooth wave increases with increased difference in those frequencies, as shown in Figs. 3(b) and 3(c).

Each domain wall movement could be observed clearly up to 5 kHz as shown in Fig. 4. However, the sawtooth inclination increases and the width of each sawtooth becomes narrow as frequency increases. Applicable frequency range for observation is limited by this factor.
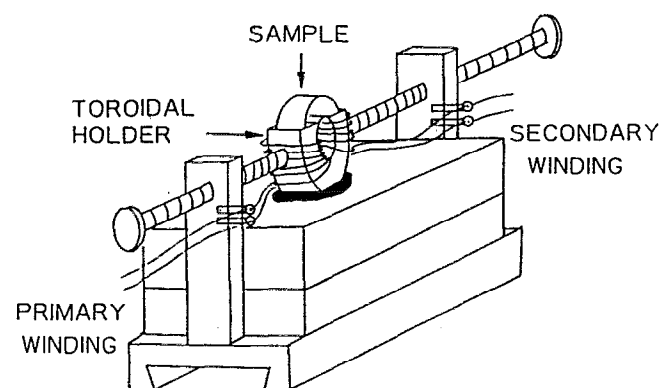
TABLE I. Dimension of the cores used in the experiment.

No.	t (μm)	b (mm)	D_m (mm)	S (mm²)	W_g (mg)
1	17	6.8	11.8	1.01	285
2	22	4.6	24.8	0.77	456

t: thickness; b: tape width; D_m: mean diameter; S: cross-sectional area; W_g: weight.

FIG. 1. Core fixture for domain observation and loss measurement.
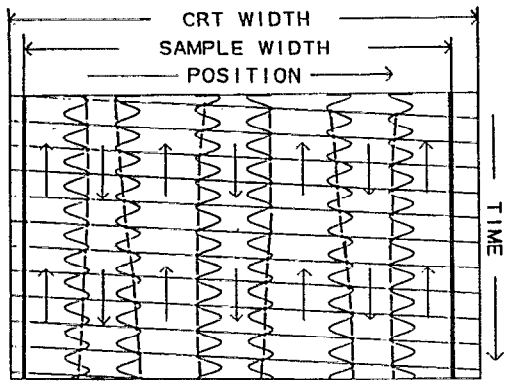
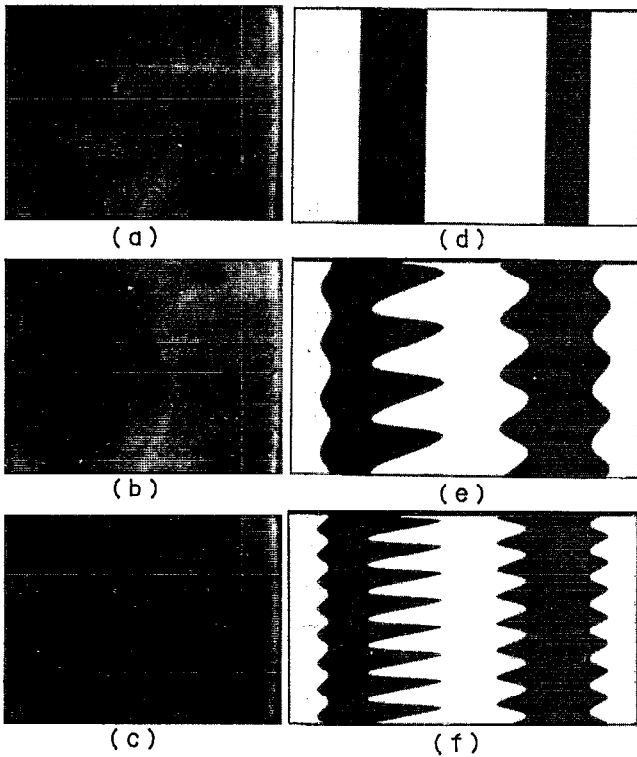FIG. 2. Explanation of the observation method of dynamic domain pattern.

FIG. 3. Variation of the observed and the simulated dynamic domain patterns against drive frequency: (a) 50.0 Hz; (b) 50.5 Hz; (c) 51.0 Hz; (d) 50.0 Hz; (e) 50.5 Hz; and (f) 51.0 Hz (scan frequency is 50.0 Hz, core No. 2).
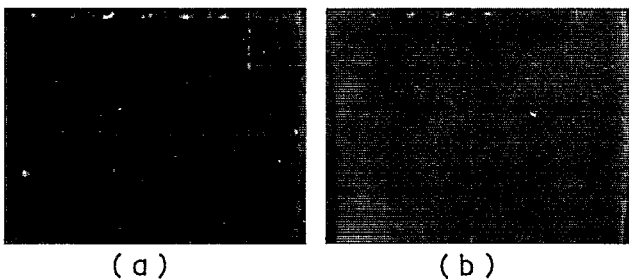

FIG. 4. Variation of dynamic domain patterns against the drive frequency: (a) 2001 Hz and (b) 5001 Hz.
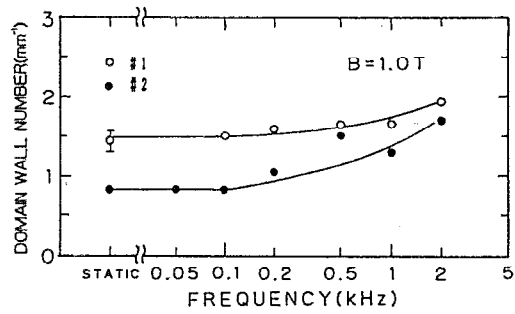

FIG. 5. Relation between the domain wall number and the drive frequency.
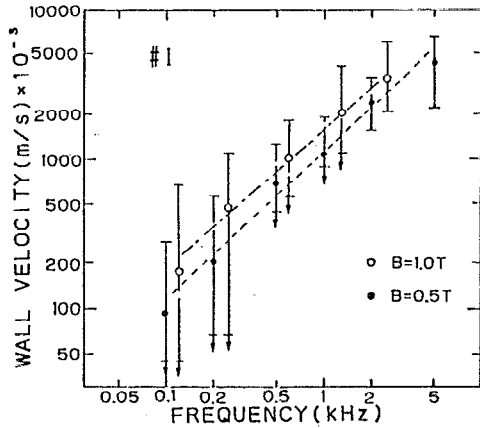

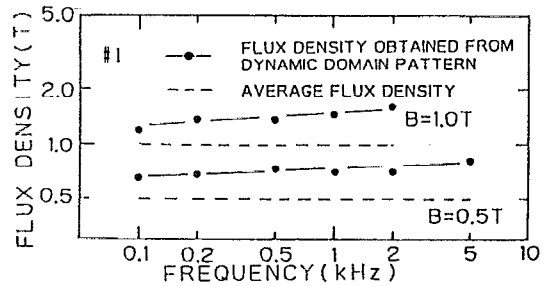FIG. 6. Relation between the wall velocity and the drive frequency.

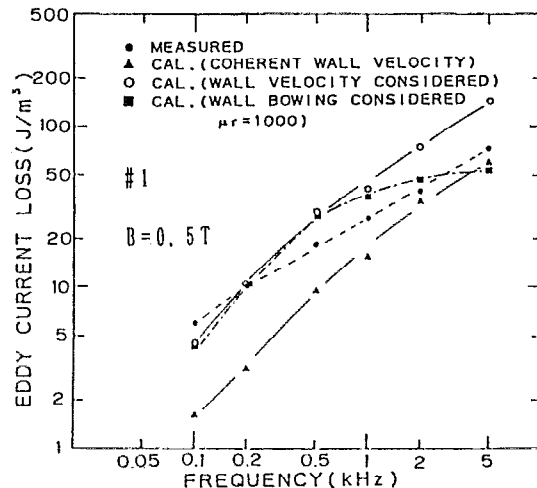FIG. 7. Comparison of average flux density with flux density obtained from dynamic domain pattern.

FIG. 8. Dependence of the eddy current loss on the drive frequency.

TABLE II. Models for the calculation of eddy current loss.

Model No.	Domain wall number	Domain wall velocity	Domain wall bowing	Expression for eddy current loss, W_e	Reference
1	obtained from observation	uniform for each wall	unconsidered	$W_e = \dfrac{8.4b\,df^2\,B_m^2}{\pi n \rho}$	(1)
2	obtained from observation	calculated from observation	unconsidered	$\dfrac{1}{bT}\displaystyle\sum_{i=1}^{N}\int_0^T \beta_{e_i} v_i^2\,dt \qquad \beta_{e_i} = \dfrac{8.4B_s d}{\pi^3\rho}$	(1)
3	obtained from observation	calculated from observation	considered	$\beta_{e_i} = \dfrac{16\,dB_s^2}{\pi^3\rho}\displaystyle\sum_{k=\text{odd}}\dfrac{1}{k^3 + 16k(2\pi L_i \mu f d/\rho)^2}$	Induced from Ref. 6

b: tape width; d: thickness; f: frequency; n: domain wall number; v_i: ith wall velocity; B_m: maximum flux density; B_s: saturation flux density; L_i: a half of ith domain wall width; β_{e_i}: viscous damping const. of ith domain wall due to eddy current; μ: permeability; ω: angular frequency; ρ: resistivity.

RESULTS AND DISCUSSION

Figure 5 shows the dependence of domain wall number on the frequency at $B = 1.0$ T. The cores were demagnetized at 50 Hz before domain pattern observations at each frequency. The domain wall number was independent of frequency below a threshold frequency of 200 Hz. Above the threshold frequency, the domain wall number increased with frequency. We found that the new domain walls were generated at the side of the sample, and that the nucleated domain wall went into the sample center direction with the increase of the drive frequency. At that time, the domains with small width were annihilated by the domains of larger width.

Figure 6 shows the dependence of the velocity of each domain wall on the drive frequency. The error bar represents the maximum and the minimum velocities of each domain wall and an arrow under the error bar means that the minimum velocity of the domain wall was zero. That is, generally, the velocity of each domain wall in the same sample differs from the others. When the drive frequency was increased, the domain wall velocities were contained in a narrower distribution. However, the maximum and the minimum velocities still differed by a factor of 3 even in the kilohertz region.

Figure 7 compares the flux densities obtained from either the dynamic domain patterns or the induced voltage of the search windings. The induced voltage gives a volume average value, and it was kept constant. The dynamic domain pattern indicates the surface flux density. Since the surface flux density increases with increasing drive frequency, wall bowing might occur even in a 17-μm thick strip.

Figures 5–7 suggest that the eddy current losses for the very thin silicon steel cores are influenced by the dynamic domain wall number, the wall velocity and the wall bowing simultaneously.

Figure 8 compares the measured eddy current losses and the calculated ones. The eddy current losses in Fig. 8 and the domain wall numbers in Fig. 5 were measured simultaneously. Three models were applied to calculate the eddy current losses and the models are explained in Table II. The main model is Model 3 which includes the contributions from the dynamic domain wall number, the wall velocity, and the wall bowing simultaneously. The domain wall number and the wall velocities were obtained from the dynamic domain patterns. The wall bowings were estimated by using the Lee's model.[6] The calculated eddy current losses agree comparatively well with the measured ones.

In the case that we neglected the wall bowing (Model 2), the calculated eddy current losses were larger than measured values. If we neglect both the wall bowing and the difference between the velocity of each domain wall (Model 1), the calculated values were less than measured ones, even though Model 1 took account of the dynamic domain wall number.

CONCLUSION

Dynamic domain pattern observation and eddy current loss measurement of tape-wound cores made of 17–22 μm thick (110)[001] oriented silicon steel strips were performed simultaneously. The major results are as follows.

(1) Dynamic domain patterns were observed using a SEM. Provided there is a slight disparity of drive frequency from scan frequency or its integral multiples, dynamic domain wall number and the velocity of each domain wall can be observed up to 5 kHz.

(2) The measured eddy current losses agreed comparatively well with the calculated one which takes account of the dynamic domain wall number, the velocity of each domain wall and the wall bowing.

[1] Y. Sakaki, IEEE Trans. Magn. MAG-16, 569 (1980).

[2] F. J. Friedlaender, Trans. AIEE 75, 268 (1956).

[3] K. I. Arai, K. Ishiyama, and H. Mogi, IEEE Trans. Magn. MAG-25, 3949 (1989).

[4] K. I. Arai, H. Mogi, and K. Ishiyama, IEEE Trans. Magn. MAG-26, 1966 (1990).

[5] K. I. Arai, H. Satoh, and K. Ishiyama, IEEE Trans. Magn. MAG-26, 1969 (1990).

[6] E. W. Lee, Proc. IEE 107C, 257 (1960).

[7] J. W. Shilling and G. L. Houze, IEEE Trans. Magn. MAG-10, 195 (1974).